Measurement of Plasma Induced Flow Perturbations Affecting a Mach 4.5 Corner Separation Zone

Brock Hedlund[1], Alec Houpt[2], Stanislav Gordeyev[3], and Sergey Leonov[4]

Institute for Flow Physics and Control, Department of Aerospace and Mechanical Engineering, University of Notre Dame, Notre Dame, IN, 46556

This study was performed to compare the effect of pulsed plasma actuators in Three Electrode Discharge (TED) and Shallow Cavity Discharge (SCD) configurations on downstream flow perturbations through the observation of the separation zone of a hypersonic boundary-layer occurring over a compression ramp surface. Tests were carried out in Mach 4.5 flow with varying Reynolds number to characterize naturally developing flow perturbations and the plasma-induced perturbations by different diagnostic tools. A high resolution Shack Hartmann wavefront sensor was used to measure flow density gradients and produce spectra of density perturbations before and during plasma actuation. High-speed schlieren imaging was able to distinguish separation of the boundary-layer and generate spectra of oscillations at the boundary-layer edge from extrapolated values of pixel intensity. Changes in the spectra of dominant flow perturbations due to plasma actuation were compared with spectra taken with high frequency PCB™ pressure sensors. The effects of plasma actuation at low (TED) and high (SCD) frequency configurations demonstrate a different pattern of interaction, appearing in a downward or upward shift of the dominant frequency of flow perturbations respectively.

I. Introduction

Many studies focused on the development of effective flow control by means of electrical discharges have been carried out previously to observe their effect on a boundary layer in subsonic and supersonic flow through multiple measurement techniques that are non-disruptive to the flow. A high sensitivity of the flow structure to the presence of mechanical obstacles limits the methods of analysis to non-intrusive optical imaging systems or flush mounted surface pressure sensors. Previously, measurements taken by Shack-Hartmann wavefront sensor and pressure transducers have provided somewhat complimentary results[1]. The goal of the present study is to further explore the influence of a pulsed plasma actuator on the spectra of flow perturbations existing in the separation zone of a hypersonic compression ramp corner and near the development of perturbations in the upstream boundary layer. Plasma actuator configurations pulsed at both high frequency (100 kHz) and low frequency (5 kHz) were employed to disturb the flow and observations were made using a correlation analysis of the Shack-Hartman wavefront sensor, schlieren images[2], and differently located surface mounted pressure sensors for comparison.

Motivation to study the oscillatory behavior of hypersonic boundary layers stems from the development of scramjet engine inlets for sustainable hypersonic flight. Crucial to the development of practical engine designs is the need for an efficient inlet, responsible for both effective compression and preconditioning of the flow for combustion. At low Re, a necessary preconditioning particularly consists of a boundary layer forcing to a turbulent state to prevent inlet unstart and mitigate flow separation originating from the SWBLI on compression surfaces. At the altitudes characteristic for scramjet operation, natural transition to turbulence within the boundary layer does not always occur in a small-scale apparatus due to a relatively low Reynolds number and flow compressibility at a high Mach number. The boundary layer can be tripped[3, 4] through the generation of a streamwise vorticity in the flow[5], leading to an acceleration of the laminar-turbulent transition. Thermal methods used to trip the hypersonic boundary layer have been previously explored both theoretically, in Ref [6] and in later works of those authors, and experimentally, in Ref [7] and references herewith.

It was shown[8] that the use of pulsed plasma actuators for the production of initial perturbations of gas pressure leads to generation of high frequency velocity disturbances in the flow due to non-uniform localized heating. It was

---

[1] Graduate Student, AIAA Student Member.
[2] Graduate Student, AIAA Student Member.
[3] Associate Professor, AIAA Associate Fellow.
[4] Research Professor, AIAA Associate Fellow.

also argued[8] that the use of plasma actuators instead of physical instruments for boundary-layer control offer many advantages, such as their thin and lightweight design, electronic control, flexibility in frequency generated, and lack of moving parts. However, typical plasma actuator designs pose a few disadvantages as well, including a limited magnitude of force production and low efficiency of momentum transfer. A recent study[9] has shown the extensive work done to characterize the controlling effect of near surface plasma discharges on airflows, including pulsed SDBD discharges used to generate a high amplitude repetitive forcing of the flow through localized heating. This method is used to promote turbulence upstream of the compression ramp corner and can be measured by means of many different diagnostic techniques. Using optical and pressure sensing methods to observe both the spatial and temporal responses can result in the determination of changes occurring in dominant perturbation frequencies present in the flow field. Many other diagnostic methods have been employed in the measurement of spatial and temporal changes in flows due to plasma actuation[10,11], however the scope of this study is limited to measurements taken by schlieren, Shack-Hartmann wavefront sensing, and high frequency pressure transducers.

Previously, the feasibility of using a Shack-Hartmann wavefront sensor to determine the dominating frequencies of flow oscillations in the flow field near a corner separation zone was experimentally proven[12]. Wavefront sensing was demonstrated to be a proper candidate for non-intrusive high frequency aero-optic measurements in hypersonic conditions due to the expectation of spanwise uniformity in flow and the sensor's sole sensitivity to gas density gradients. In addition, the wavefront sensor is capable of providing high spatial resolution and up to 1 MHz frequency response, limited only by the imaging camera's technical capability.

Schlieren visualization is a widely used technique for imaging the density gradients of a flow field. Generally for a simple schlieren setup it is difficult to back out any quantitative data about flow parameters. However it is possible to extract the frequencies at which the density gradients are oscillating. There are two ways of doing this: 1. Take a line profile in the region of interest, find the associated wavenumbers, and then transform them into the frequency domain. 2. Use a high-speed camera to capture images and find the time profiles of the value of certain pixels in the image.

The limitation to these optical methods is that they are unable to measure gas disturbances directly at the surface, however due to the configuration of this model (see Fig. 1) surface pressure measurements can be made through the use of surface mounted sensors. The measurement of high frequency pressure perturbations in a hypersonic boundary layer by means of surface mounted pressure sensors has been employed experimentally by Raman[13] and Estorf[14], for example. Using 1 MHz response PCB sensors, pressure perturbations along the surface of a model in a hypersonic boundary layer can be detected and analyzed spectrally.

II.　　Experimental Approach

A.　Facility

Testing was performed in the ACT-1 hypersonic wind tunnel of the University of Notre Dame. The facility is equipped for testing at Mach 4.5 and 6 through nozzle arrangements. Capabilities for this tunnel also include an arc heater for generation of high enthalpy flows up to 6 MJ/kg to simulate the flow conditions close to ones typical for hypersonic flight. This corresponds to a stagnation temperature $T_0 > 800\ K$ and up to 4000 K (high enthalpy) or $T_0 = 293\ K$ (low enthalpy). Other relevant test conditions include Reynolds Number $Re_L > 3 \cdot 10^6\ m^{-1}$ (low enthalpy) or $Re_L > 4 \cdot 10^5\ m^{-1}$ (high enthalpy), and stagnation pressure $5.5\ bar > P_0 > 0.8\ bar$. The composition of the gas mixture (typically nitrogen or artificial air) is controlled through variation of pressures and arrangement of the injection ports.

The experimental configuration for testing includes a compression ramp model mounted in the test section of ACT-1 (see Fig. 1). The experimental model consists of a flat plate with a sharp leading edge and lower surface at a fixed angle $\alpha = 15°$. The second wedge is interchangeable and is mounted on top of the flat plate to form the compression ramp at angles $\beta = 20° - 25°$. Ramp angles varied, with the 20° ramp being used in the TED configuration and the 25° ramp in the SCD configuration. In total, the model measures: length $L = 229\ mm$, width $W = 102\ mm$, and height $H = 19\ mm$. Also shown in the figures is the arrangement of PCB 132 series sensors in the model. With a response frequency of 1 MHz, these piezo-electric transducers are capable of detecting weak shocks and high frequency perturbations impacting the surface. They are flush mounted at the locations labeled CH1, CH2, and CH3 in Fig. 1 to provide measurements on the surface of the flat plate in both the boundary layer and within the separation bubble. At the locations labeled K1 and K2 in Fig. 1a, lower frequency pressure measurements were made by Kulite™ XT-140 series subminiature pressure transducers.
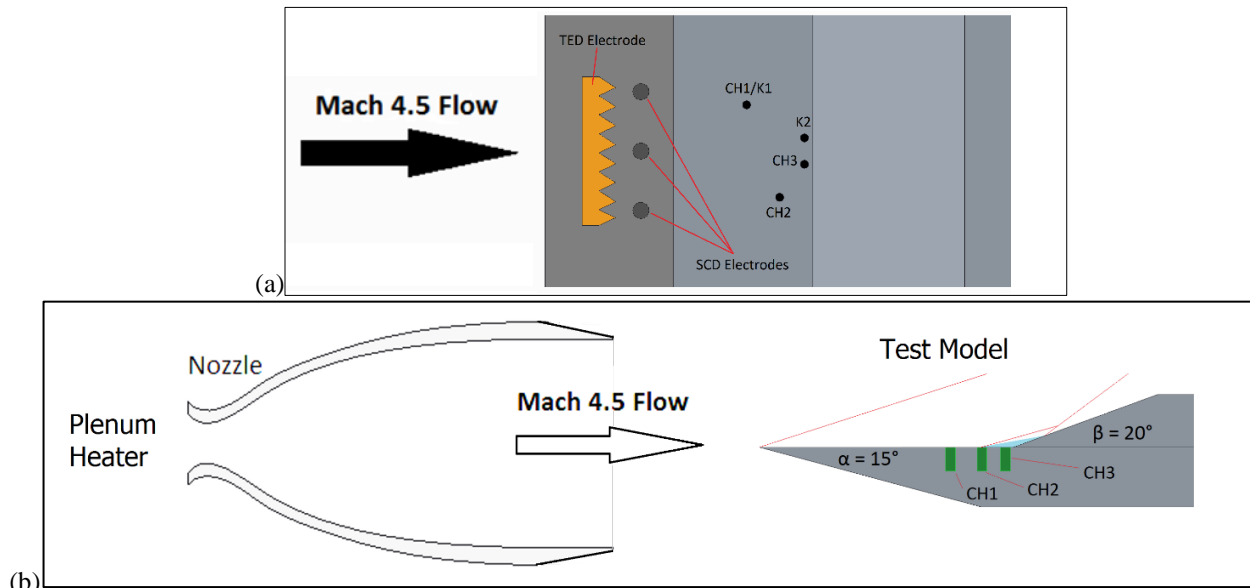
2

Figure 1. (a) Top down view and (b) side view of test model

Aero-optical measurements were performed using a high-speed Shack-Hartmann wavefront sensor[15]. The system consisted of a laser beam expanded to a 50-mm-diameter collimated beam and passed along the spanwise direction over the corner region of the model mounted in the test section. The spanwise beam propagation was chosen for two reasons. First, the flow is expected to be primarily spanwise-uniform. Second, as the beam traverses the 4-inch-long region of the flow, aero-optical distortions become stronger thus improving the signal-to-noise ratio[16]. After exiting the test section, the beam is reflected off the return mirror, which sends the beam back along the same path. This so-called double-path setup further amplifies the aero-optical signal by a factor of two, as the beam traverses through the flow of interest twice, and also simplifies the optical setup. The returning beam is split off using a cube beam splitter, sent though a contracting telescope, which reduces the beam size to 12.5 mm in diameter, and recorded by a Phantom v1611 high-speed digital camera. The camera had a 38 mm focal length, 70×60 lenslet array with 0.3-mm-pitch with 100% fill ratio, attached to it. After passing through the lenslet array, the beam was split into subaperture beams and focused on the camera sensor, creating a series of dots. To achieve the high, 531 kHz, sampling rate, only a small portion of the image (128×64-pixel) was acquired for the full duration of the tunnel run.

A high-speed schlieren system was used to study the flow field near the corner. Images were taken at a rate up to 30 kfps with a Photron FastCam Ultima APX. A high-intensity fiber optic continuous white light source provided the necessary illumination to image at such high frame rates. An adjustable focal length lens was used to focus on the middle of the test surface. All relevant flow images were processed using background correction by subtraction of an average image without flow. Fig. 2a shows a sample schlieren image of the flow field and its relevant features gathered at 8 kfps. In order to increase the frame rate the size of the image had to be reduced. The corner separation area was imaged at 30 kfps and is shown in Fig. 2b.
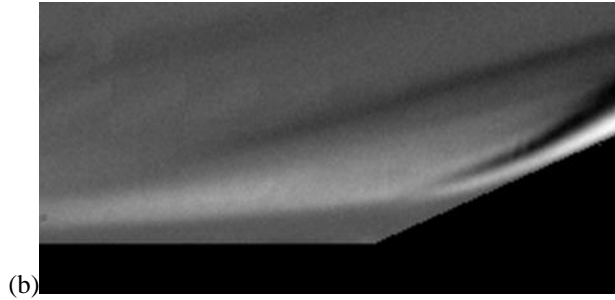
(b)
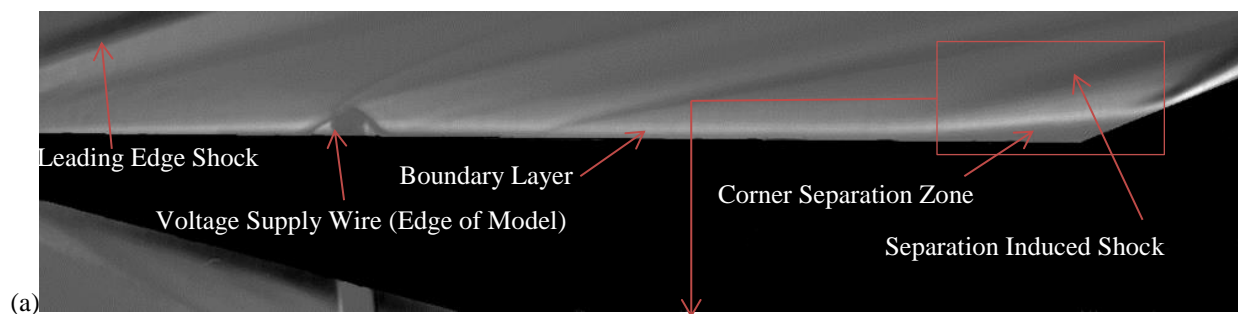
Figure 2. Background corrected schlieren image of typical M=4.5 flow without plasma actuation (Re = 2.13x10^{7}/m). (a) – 8 kfps (1024×256 pixels); (b) –30 kfps zoomed in on the corner (256 ×128 pixels)

B. Plasma Parameters

Two types of electrical discharges were tested for the control of the separation zone at the compression ramp: the Three-Electrodes Surface Discharge (TED)[17,18] and the Shallow Cavity Discharge (SCD)[19]. A scheme of the TED discharge is shown in Fig. 3. This type of discharge employs a dielectric barrier discharge for an initial ionization of air an then a pulsed direct current waveform for an additional energy deposition, as it is shown in the time series, Fig. 4 measured in M=4.5 flow. A short pulse repetitive operational pattern is used to prevent an arcing process. The shape of the high-voltage electrode was a rounded strip or a saw-tooth strip. The TED discharge parameters are summarized below.
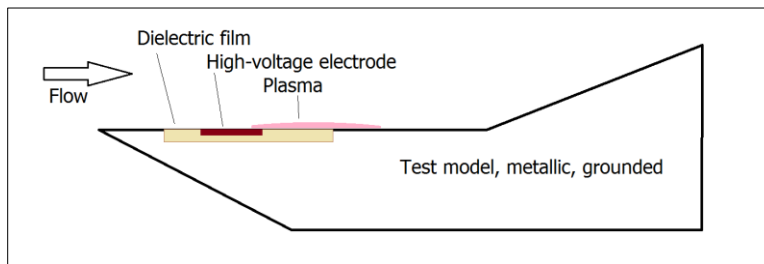

Figure 3. Principal schematics of TED electrical discharge.

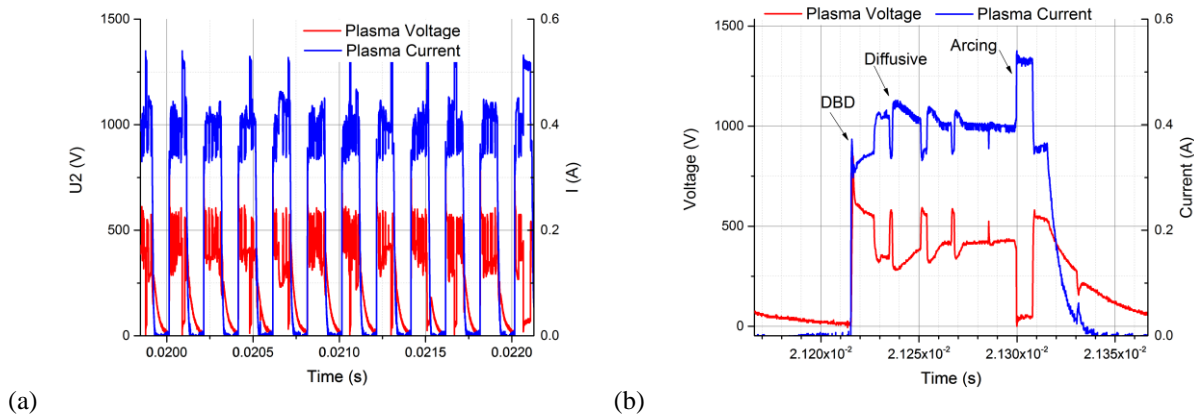(a)   (b)

Figure 4. (a) Time series of operation; (b) details of the individual pulse.

Discharge parameters:

- voltage applied   up to 2 kV
- frequency of repetition   up to 5 kHz
- discharge duration   0.04-0.1 s
- duty cycle   0.5
- typical mean power   80 W

4

The generation of a plasma sheath occurs in a thin layer just above the model surface, acting as a thermal actuator to trip the flow. The experimental model with a rounded strip is shown in the photo in Fig. 5a; the discharge image with the saw-tooth strip is shown in Fig. 5b.
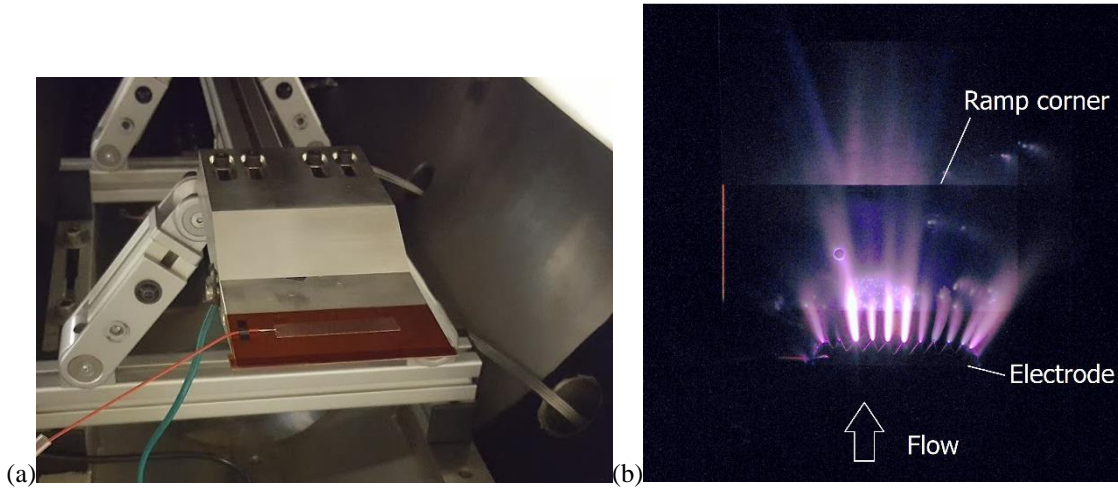

Figure 5. Images of (a) TED rounded strip configuration; (b) generation of plasma along the model surface – top view.
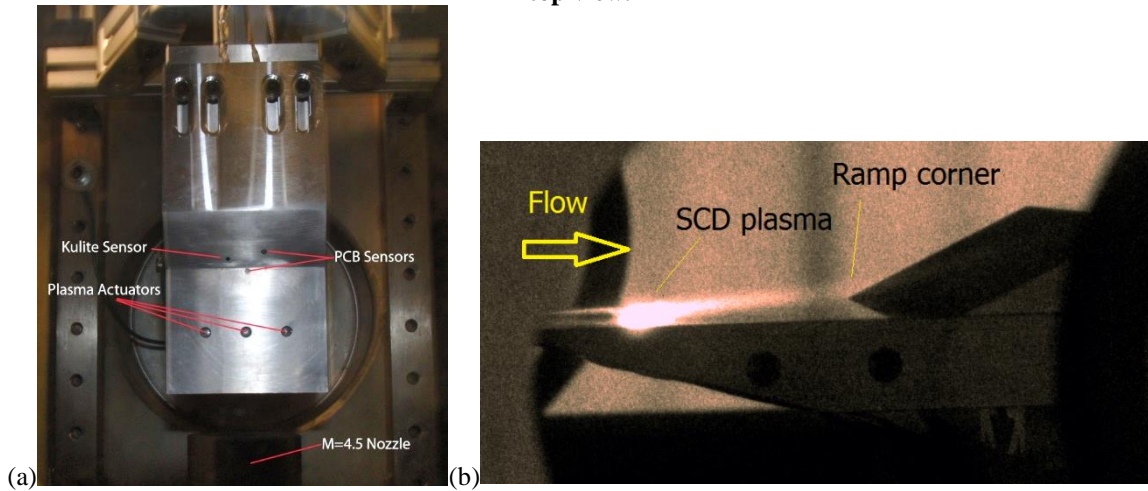

Figure 6. (a) Model with the SCD in the test section of ACT-1 at the University of Notre Dame; (b) the SCD image in M=4.5 airflow – side view.

Three shallow cavity discharge (SCD)[1,20] plasma actuators mounted in the flat plate are arranged spanwise and flush to the model's upper surface 62 mm upstream of the ramp corner, as it is shown in Fig. 6a. These actuators function in a push-pull mode with pulsing frequencies much higher than one for the TED. They operate at a reasonably low voltage and are capable of producing disturbances of required magnitude within the flow field for observation. The time series of the SCD operation in M=4.5 airflow is shown in Fig. 7a for a frequency of repetition $f = 100\ kHz$. The pulse energy and average power were calculated based on these data, as it is shown in Fig. 7b.

5

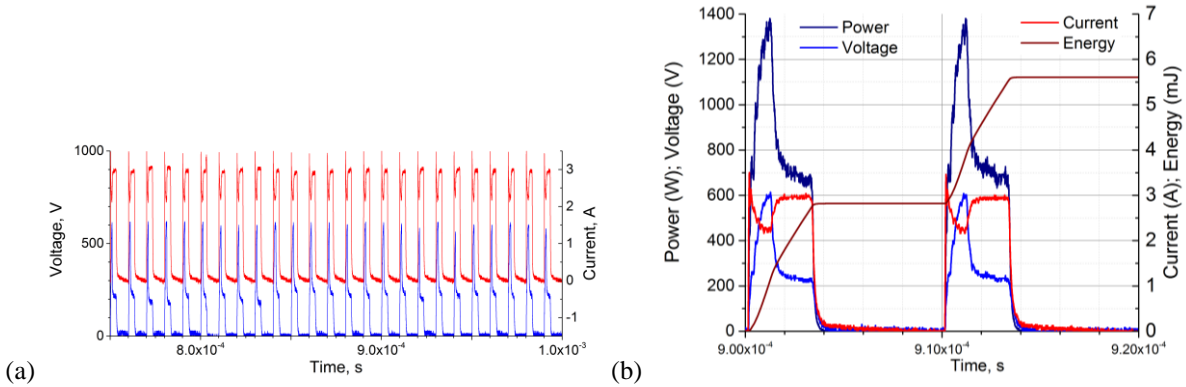(a)   (b)

Figure 7. (a) Voltage – current time series of the SCD operation at $f = 100\ kHz$; (b) calculation of the discharge pulse power and energy for 3 SCDs.

The discharge parameters were as follows:
- voltage applied   up to 1 kV
- frequency of repetition   up to 100 kHz
- discharge duration   0.04-0.1 s
- pulse energy   0.8-1.2 mJ/unit
- duty cycle   0.2-0.5
- typical mean power   300 W

III.   Experimental Data

A.   Flow Characterization

Tests were conducted to measure the freestream speed directly behind the nozzle exit for hot and cold flow conditions with the Shack-Hartmann wavefront sensor. For this measurement, the laser beam was sent normal to the flow direction just downstream of the nozzle at the centerline. At a sampling rate of 530 kHz, the beam deflection angles were measured on a rectangular grid consisting of 10 points in the streamwise direction and 5 in the radial. Using a multi-point cross-correlation technique[21], the deflection angle power spectra, phase difference between adjacent streamwise points, and corresponding convective speeds at several points were calculated. It is important to note that these measurements are directly from the convective speeds of optically-active small scale turbulence structures occurring naturally in the freestream.

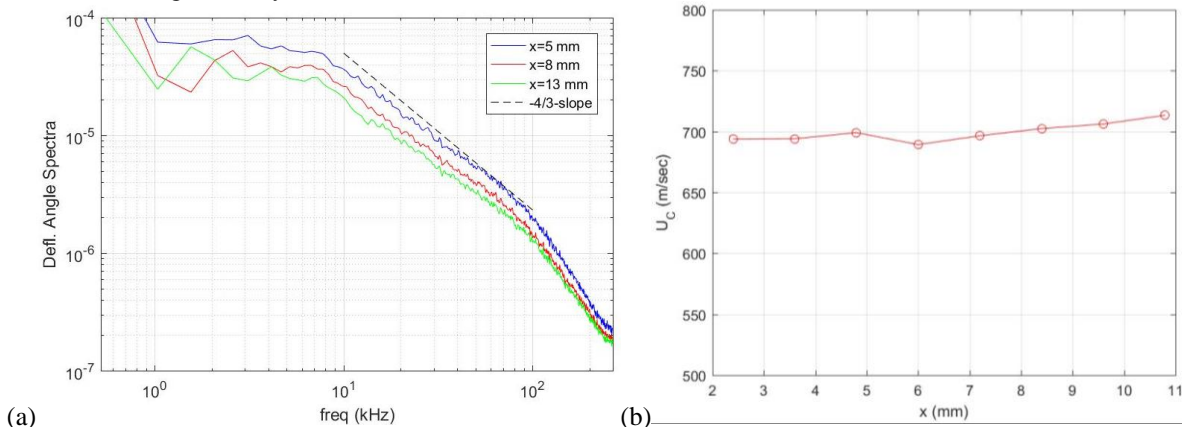(a)   (b)

Figure 8. (a) Deflection angle spectra and (b) freestream velocities measured by SH sensor at different streamwise locations measured from the nozzle edge for the T0 = 300K case.

At different streamwise points in cold flow, the extracted deflection angle power spectra is shown in Fig. 8a. Indicating a consistency with the decaying process of isotropic turbulence, there is a decay in the streamwise direction of the spectra. A power slope of -4/3 can be seen in all spectra between 10 kHz and 100 kHz. This is represented by a

6

dashed line in Fig. 8a. Previously, it was shown in Ref[22] that in the self-similar energy transfer region, this indicates Kolmogorov-type turbulence. Isotropic turbulence is also present in the freestream immediately behind the nozzle.

The direct measurements of freestream convective velocity during a cold flow test are shown in Fig. 8b varying with streamwise location. Immediately after the nozzle, the velocity is approximately 700 *m/s*. Calculations of freestream speed for conditions at M = 4.5 and $T_0 = 300$ *K* by means of isentropic relations also give a value of 700 *m/s*. Expansion of the flow into the vacuum chamber results in the formation of an under-expanded jet with speed increasing slightly with distance downstream, which can be seen in Fig. 8b. These results indicate that when small scale turbulence is present, measurements made with a Shack-Hartmann wavefront sensor prove to be applicable for the direct measurement of flow properties. In the case of hot flow, the flow density drops by a factor of up to 5, comparing to cold flow, this results in a reduction of optical distortions by about the same ratio. Careful analysis of the convective flow velocity measurements taken in hot flow indicates a freestream speed ranging from 1,100 to 1,400 *m/s*, with estimated total temperature to be between 800 and 1250 *K* (See Table 1).

Table 1. Flow characteristics for cold and hot flow in ACT-1 (isentropic estimate based on freestream velocity measured by aero-optical method)

Cold			At Nozzle Exit					
P0 (bar)	Mass Flow (kg/s)	T0 (K)	T (K)	Velocity (m/s)	a (m/s)	P (Pa)	ρ (kg/m^3)	Unit Reynolds (1/m)
1.5	0.037	293	58	699	155	518	0.030	7.1E+06
1.9	0.048	293	58	699	155	656	0.038	9.0E+06
2.5	0.060	293	58	699	155	864	0.050	1.2E+07
3.2	0.078	293	58	699	155	1106	0.064	1.5E+07
4	0.096	293	58	699	155	1382	0.080	1.9E+07
5.5	0.134	293	58	699	155	1900	0.110	2.6E+07
Hot			At Nozzle Exit					
P0 (bar)	Mass Flow (kg/s)	T0 (K)	T (K)	Velocity (m/s)	a (m/s)	P (Pa)	ρ (kg/m^3)	Unit Reynolds (1/m)
1.5	0.020	1238	245	1437	319	518	0.007	6.7E+05
2.25	0.032	906	179	1229	273	777	0.015	1.5E+06
3	0.043	880	174	1211	269	1037	0.020	2.1E+06
3.25	0.049	835	165	1180	262	1123	0.023	2.5E+06

Three PCB™ 132A31 pressure sensors were used to provide measurements of the flow pressure perturbations along the model surface. The sensors were located upstream of the ramp corner, with the sensing element mounted flush to the model's top surface. Along the flow axis, the sensors labeled CH1, CH2, and CH3 were mounted 20 mm, 10 mm, and 2.5 mm upstream of the ramp corner, respectively, that is illustrated in Fig. 1. This spacing allowed for measurement of the flow pressure perturbations in the corner separation zone (CH3), near the flow separation point (CH2), and within the boundary layer upstream (CH1). Schlieren images verify the location of separation and existence of the separation zone within the corner. The sensors and their cables were carefully insulated to reduce vibrational noise from the model and electromagnetic noise from surrounding electronics.

Across a range of Reynolds numbers, each pressure measuring channel exhibits slightly different dynamics due to differences in their locations. For cold flow tests, shown in Fig. 9, the progression downstream from channel 1 to channel 3 indicates a growth in perturbation amplitudes, corresponding to a growth in instabilities propagating downstream. Also, very evident is the presence of a large peak at 115 kHz in Fig. 9c, measured in the separation zone. This may indicate the presence of a dominant perturbation frequency not seen in the boundary layer measured at channels 1 and 2. Across all channels in Fig. 9, there also appears to be an increase in the peak frequencies with an increase in Reynolds number. This was analyzed and a nearly linear correlation between the increase in Reynolds number and peak frequency was found.
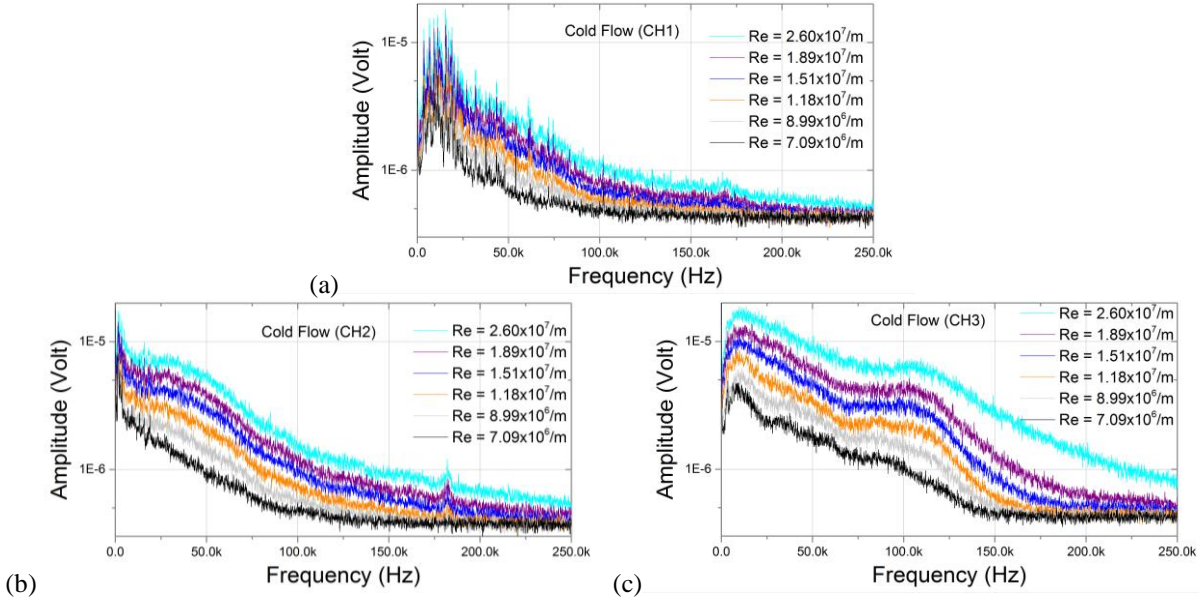
Figure 9. Spectra of pressure perturbations in cold flow over a 20° ramp for the following locations: (a) CH1 – boundary layer; (b) CH2 – near flow separation line; (c) CH3 – in separation zone.

In the case of hot flow, the signal-to-noise ratio appears to be a rather high comparing to the cold flow. The sensors detected high electromagnetic noise levels during arc operation, leading to a high noise floor in the spectra and unwanted spikes in many cases. Within the boundary layer, pressure channel 1 made almost no distinction of high frequency peaks within the spectra. However, within the separation zone, there is indication of a dominant perturbation frequency, which is shown in Fig. 10c. This bump at 140 kHz grows exponentially with Reynolds number, similarly to the observed event in aero-optical measurements. The CH2 sensor indicates an amplitude rise in the higher Re cases as well, being mounted in a region that may be passing in and out of the separation zone as it changes in size.
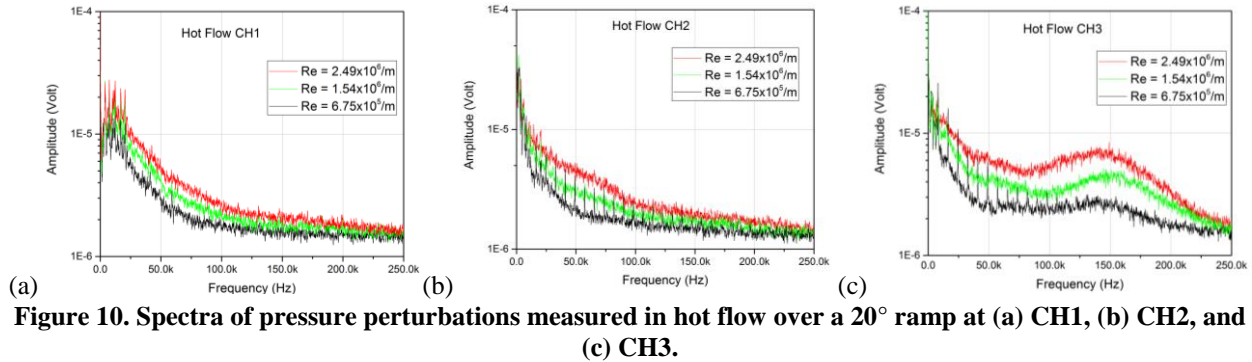

Figure 10. Spectra of pressure perturbations measured in hot flow over a 20° ramp at (a) CH1, (b) CH2, and (c) CH3.

Considering linear stability theory, naturally occurring disturbances that are most amplified over the model boundary-layer can be estimated for a flat plate. These estimations were previously carried out in Ref[1], and predicted dominant frequencies existing on the plate to be $f \approx 25\,kHz - 55\,kHz$ for unit Reynolds numbers ranging from $3.0 * 10^6\,/m$ to $8.0 * 10^6\,/m$. These estimations assumed an approximate adiabatic wall for low enthalpy tests. For high enthalpy tests, a non-adiabatic wall assumption predicted higher disturbance frequencies due to a thinner boundary-layer. The conclusion in Ref[1] however, was that these dominant frequencies were undetected by the experimental methods employed, therefore the appearance of these first mode (Tollmien-Schlichting) waves was not observed. There may be several factors contributing to the inability to detect those waves, such as (1) The high levels of acoustic and electromagnetic noise present in the facility; (2) A relatively high level of initial flow disturbances; and (3) The length of the model may not allow for the development of high enough Reynolds numbers to produce high amplitude perturbations.

8

If acoustic instabilities are considered, the previous predictions made in Ref[1] were dominant frequencies of $f = 49\ kHz$ for low enthalpy flow (assuming the boundary-layer is the same temperature as $T_0 = 300K$), and $f = 127\ kHz$ for high enthalpy flow. There can be some shift due to nonadiabatic wall conditions for hot flow, but the trend remains relatively close. Looking back to Fig. 9c, at the downstream location where the development of higher magnitude flow perturbations have shown the greatest presence in cold flow. The experimental data at highest Re does not align well with this prediction, however the shift in dominant frequency downward with lower Re conditions leads to closer alignment. In the case of hot flow, the bump indicating a dominant frequency only appears slightly higher than the predicted acoustic value.
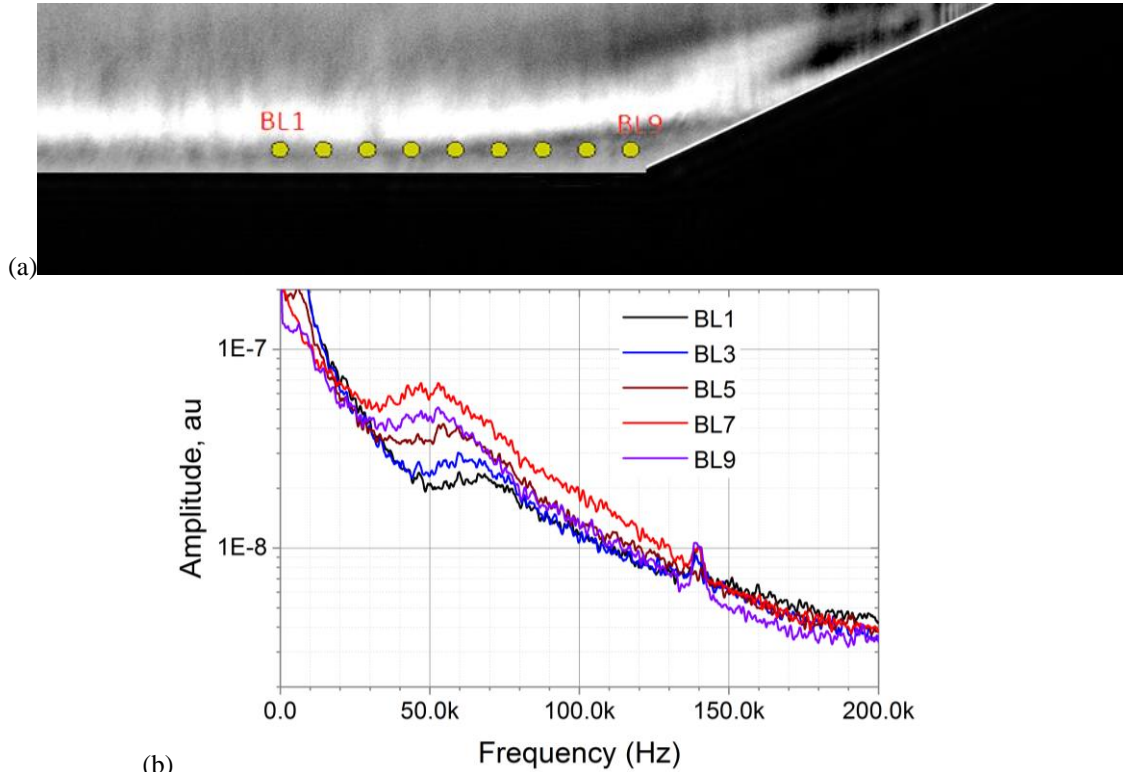

(a)

(b)

Figure 11. (a) Location of Shack Hartmann data collection points over the 25° ramp and (b) measured spectra of perturbations.

In Fig. 11b, the spectra of density perturbations show a trend of natural dominant frequency dependence on streamwise location in the flow at a unit Reynolds number of $4.3*10^6$/m. Not only does the amplitude appear to increase downstream, but dominant frequencies at the downstream locations are also lower. As the fluctuations grow in amplitude, the frequency of their oscillations reduces in turn. Closer alignment of these measurements to acoustic predictions may be due to the apparent increase of the separation zone thickness in the case of the ramp angle of 25°, compared to the data collected at an angle of 20° presented in Fig.9.

With the dominant natural frequencies present in the boundary layer and separation zone determined under these test conditions it was then possible to study the effect of pulse-repetitive TED and SCD operation on the spectra of flow perturbations in and near the corner separation zone. Deflection-angle spectra obtained using the high-speed Shack-Hartmann wavefront sensor were analyzed at the locations indicated in Fig. 11a. Early results showed[23] that SCD operation affects the spectra only slightly if the repetition frequency is less than the dominant frequency of the first-mode instability, $F_1 = 60 - 80\ kHz$. Operating at a frequency greater than F_1 produces significant changes in the spectra of disturbances.

For lower frequency pressure measurement, two Kulite XT-140-10D sensors were mounted in the surface of the model at the streamwise positions labeled as K1 and K2 in Fig. 1. This allowed for measurement of the absolute pressure dynamics in the boundary-layer and within the separation zone at up to 50 kHz. Pressure amplitude measurements by these sensors give pressure dynamics in the boundary layer (Fig. 12a) and separation zone (Fig. 12b). The flow pressure profile represented in Figs. 12a and 12b help one to visualize the time sequence of gas flow

9

and low frequency plasma actuation. The time sequence begins with the flow of nitrogen starting at *t = 0.11 seconds* and lasting for approximately 500 ms. Pulsed plasma actuation begins at 0.2 seconds and occurs for 100 ms. Looking at the pressure signal closely during plasma actuation in Fig 12c, the sensor response to plasma pulses can be seen. Since the plasma pulses last 100 microseconds, periods of higher amplitude fluctuations lasting 100 μs can be seen, followed by periods of little fluctuation.
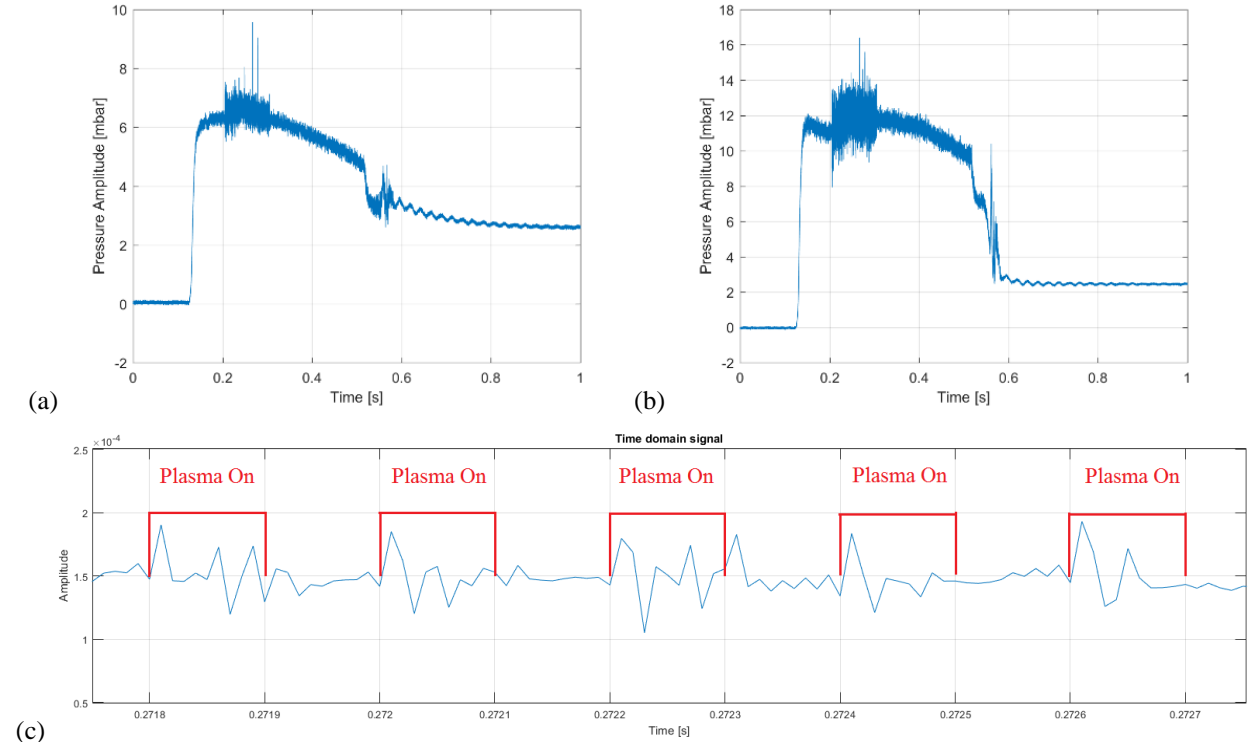

(a)

(b)

(c)

Figure 12. Pressure dynamics at location (a) K1, (b) K2, and (c) zoomed sensor response to plasma actuation in the case of installed TED.

B. Low Frequency Plasma Actuation

Schlieren images are generally considered to be qualitative data. However, fluctuations in the positions of certain flow structures can be distinguished and with time-resolved data the perturbation frequencies can be determined. A line profile was taken at the same location for every schlieren image within the flow duration. Due to the background correction, each image did not have the same intensity. An average value for the solid wall of the test model was calculated and then each line profile was adjusted to have this value by adding or subtracting a value. Fig. 13 shows the final line profiles gathered for a singular test before and during plasma actuation where each color line represents a different schlieren image. It is challenging to analyze the movement of flow structures due to the poor spatial resolution used for the higher imaging rate. However, the pixel intensity is on a 16-bit scale and provides a much more highly resolved set of data. The frequency at which the pixel intensity changed at a single pixel location was analyzed at the edge of the separation zone and at the separation related shock and is shown in Fig. 15. Fig. 14 is the time series of single pixel intensity values for the relevant portion of a run showing before, during, and after plasma actuation. There is some detectable difference in the magnitude of fluctuations during plasma actuation in Fig. 14a (still present in Fig. 14b but not as distinct).
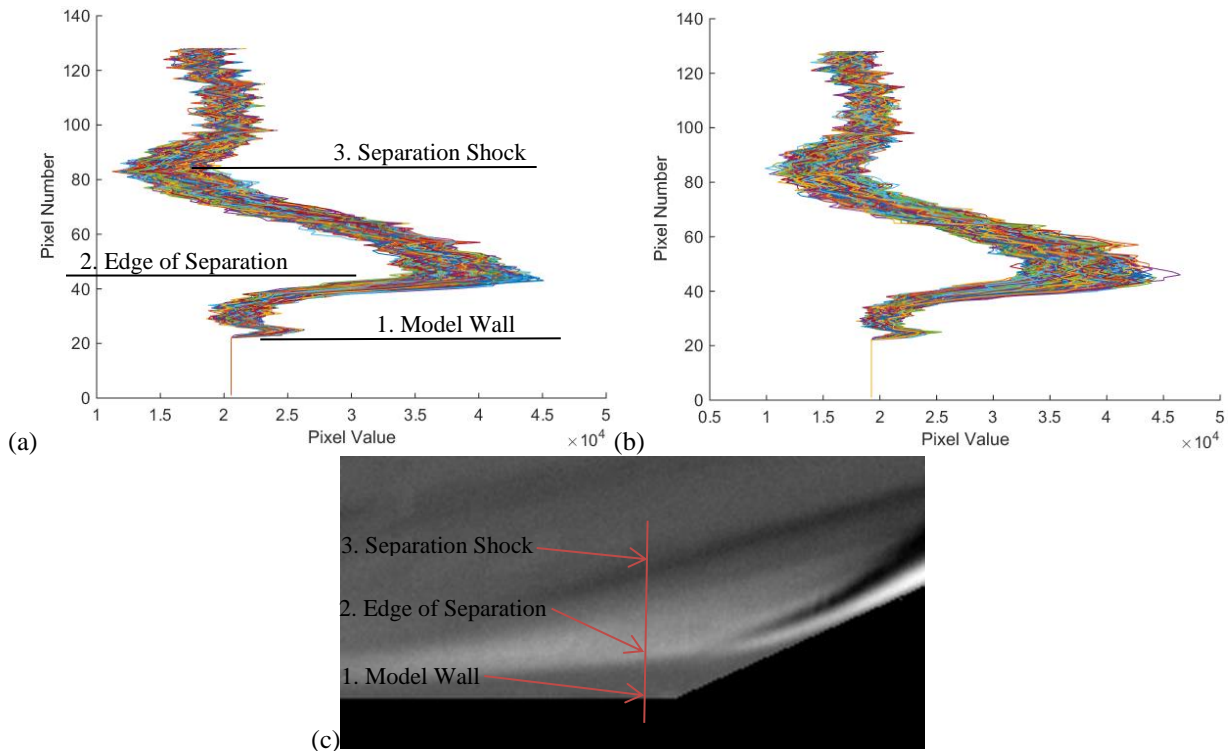
10

Figure 13. Pixel intensity line profiles: (a) before plasma actuation, (b) during plasma actuation, and (c) image depicting location of data analysis
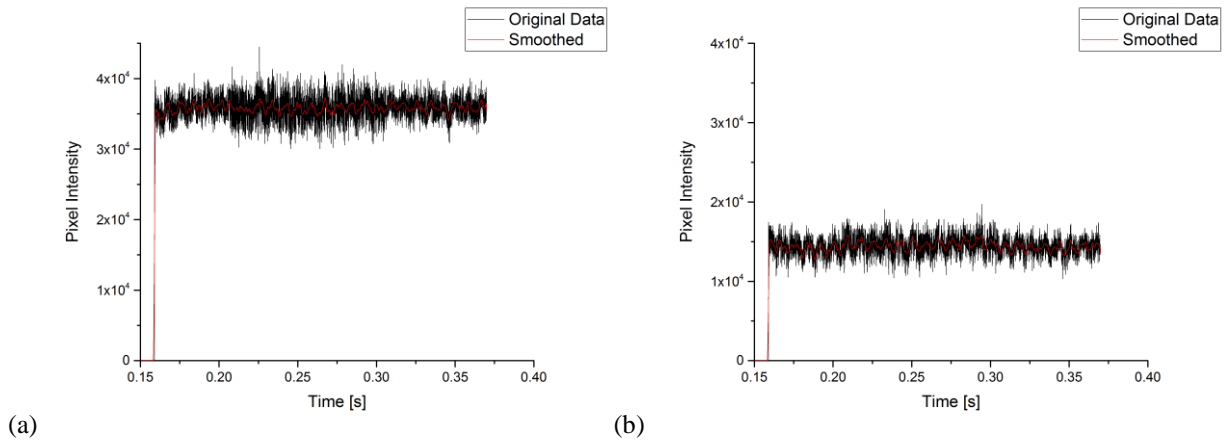

Figure 14. Single pixel intensity time series for length of test: (a) edge of separation zone; (b) separation related shock

11

(a)   (b)
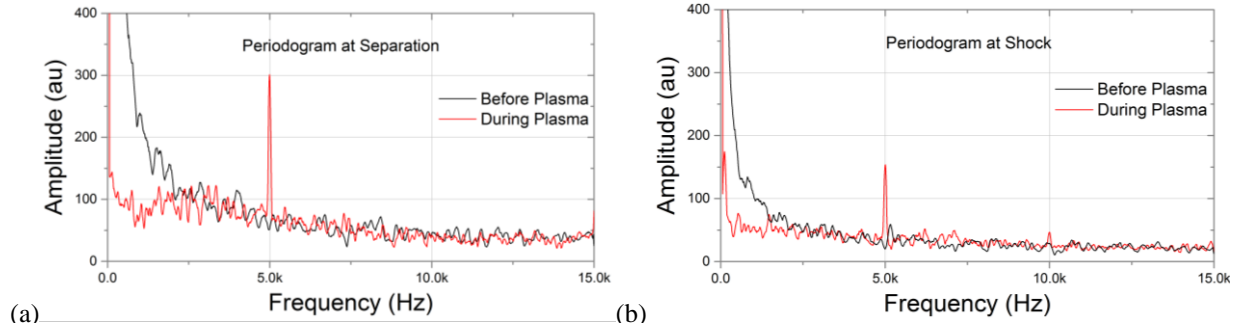
Figure 15. Frequency domain of the pixel intensity before and after plasma: (a) edge of separation zone; (b) separation related shock.

The spectra of pixel intensity fluctuations at each point indicate a few notable things in Fig. 15. First, is that both pixel locations show a significant reduction in low frequency fluctuations below 2 kHz. Following the theory of Kolmogorov's spectrum of energy distribution, these fluctuations carry the majority of energy within the turbulent flow. The second notable feature is an abrupt spike at 5 kHz, this is likely the detection of the illumination from plasma filaments by the schlieren camera.

Spectra of PCB pressure data for low frequency pulsed plasma tests are shown in Fig. 16. Pressure data was collected at three locations marked CH1, CH2, and CH3 along the compression ramp surface. Spectra of signals at CH1 and CH2 indicate very little presence of dominant perturbation frequencies both with and without plasma actuation. These trends are consistent with the tests of cold flow with ranging Reynolds numbers shown in Fig. 9a and b. The location of these sensors indicate that the presence of perturbations oscillating at any dominant frequency at these upstream positions may be negligibly small or non-existent. However, in CH2, it can be seen that a peak just below 100 kHz begins to take shape. This peak is then fully present in the CH3 signal when plasma is off (Fig. 16c). It is apparent that in all three signals, noise levels in the sensors increase greatly with plasma actuation due to the highly sensitive nature of these sensors to acoustic and EM noise. This results in the raising of the noise floor of each signal during plasma operation. What can be seen however is the shift in the dominant frequency in the pressure signal located in the separation zone (CH3) in approximately 45 kHz to the left on the spectrum (see Fig. 16c) during plasma operation. One possible explanation for this reduction in frequency may be that the separation zone is experiencing an increase in size due to expansion caused by heating of the flow during plasma operation.
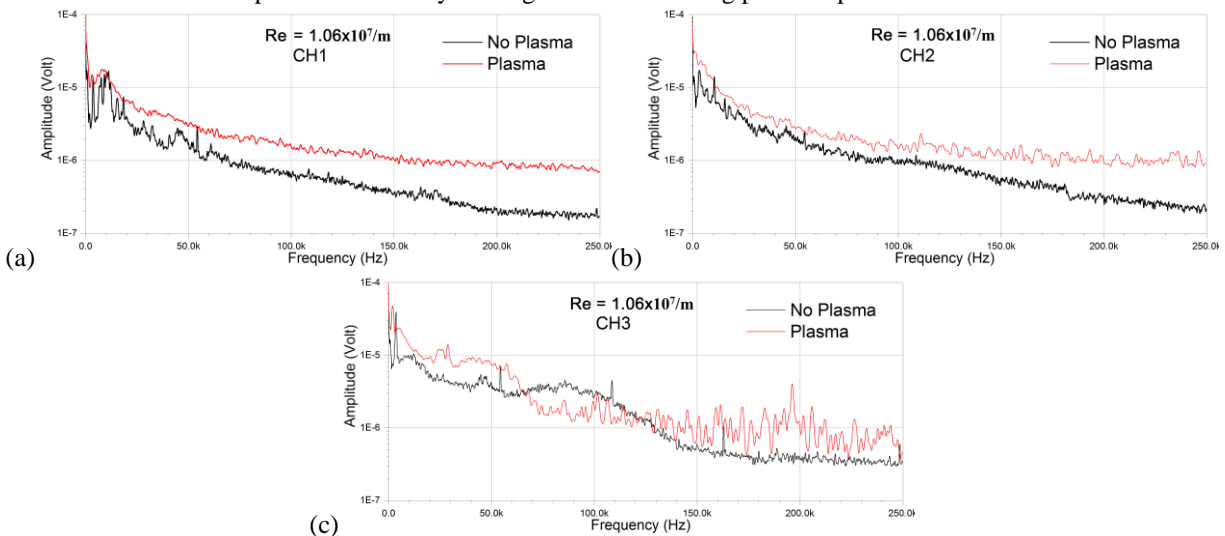

(a)   (b)

(c)

Figure 16. Spectra of pressure perturbations at (a) CH1; (b) CH2; and (c) CH3

At higher unit Reynolds numbers, the effect of plasma actuation at the separation zone location is shown in Fig. 17. In Fig. 17a, the shifting effect appears to exist still, however the peak decreases by only approximately 15 kHz. In the highest unit Reynolds number case, shown in Fig. 17b, plasma seems to have no visible effect on the frequency of dominant perturbations. The effect of varying Reynolds number on the magnitude of this shift might be explained by considering the plasma power. The existence of a "competition" between plasma power and flow enthalpy would

12

explain a smaller effect by plasma actuation at higher Re. When Re is increased, the relative plasma power is decreased in respect of the flow enthalpy. This trend will need to be verified with more datasets, however. Once again, these results seem to be in closer alignment with acoustic wave scales for this apparatus than with frequencies given by first mode wave predictions.
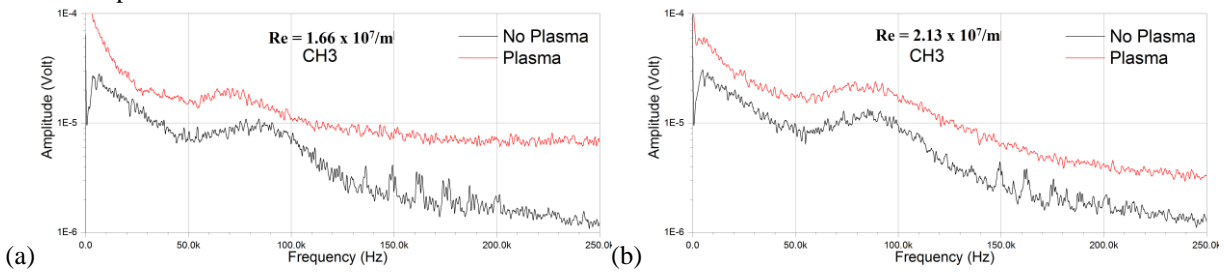

(a) (b)

Figure 17. Spectra of pressure data in the separation zone at (a) Re = 1.66 x 10^7/m and (b) Re = 2.13 x 10^7/m

C. High Frequency Plasma Actuation

As previously mentioned, the wavefront sensor takes measurements of the horizontal (X) and vertical (Y) components of the wavefront gradient. In general, equal magnitudes of vertical and horizontal wavefront gradients are expected for isotropic flows. In this study however, the flow is expected to have larger magnitudes of deflection angles in wall-normal (Y) direction in relation to the streamwise (X) direction due to larger density gradients in the wall-normal direction. The resulting effect is the generation of larger magnitude deflection angles because the effect plasma has exciting higher frequency disturbances is amplified. The measuring locations are indicated in Fig.18.
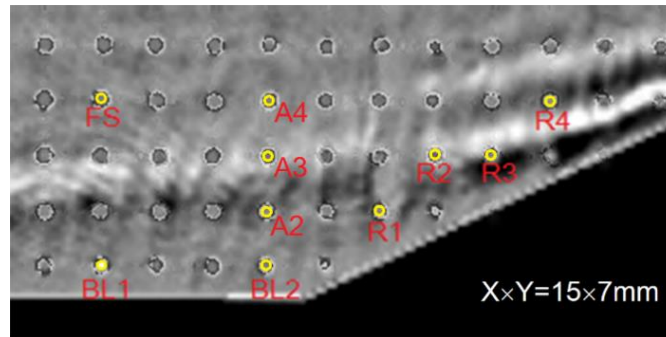

Figure 18. Shadowgraph and measurement locations

Figures 19a-d show data for plasma actuation with the SCD configuration at a frequency of $100\ kHz$ for two points in the incoming boundary layer and two points near the 25° compression ramp indicated in Fig. 18 as BL1, BL2, R1, and R2 correspondingly. Each test included measurements of $0.1\ s$ prior to plasma actuation, $0.1\ s$ during plasma operation, and 0.1s after the plasma turned off (the latest is not shown in the graphs). There appears to be a small effect due to the plasma in the boundary layer at point BL1. At the point BL2 in Fig. 19b, the amplitude of perturbations is higher and the amplitude of high-frequency disturbances larger than $80\ kHz$ increases during plasma actuation. However, looking at Fig. 19d gathered on the ramp, it can be seen that these high-frequency disturbances were excited at the cost of a significant reduction of the peak frequency oscillations. Across all sensor locations in Fig. 19, a consistent rise in the "plasma on" data indicates the excitation of perturbations at a frequency slightly higher than the natural dominant frequency.
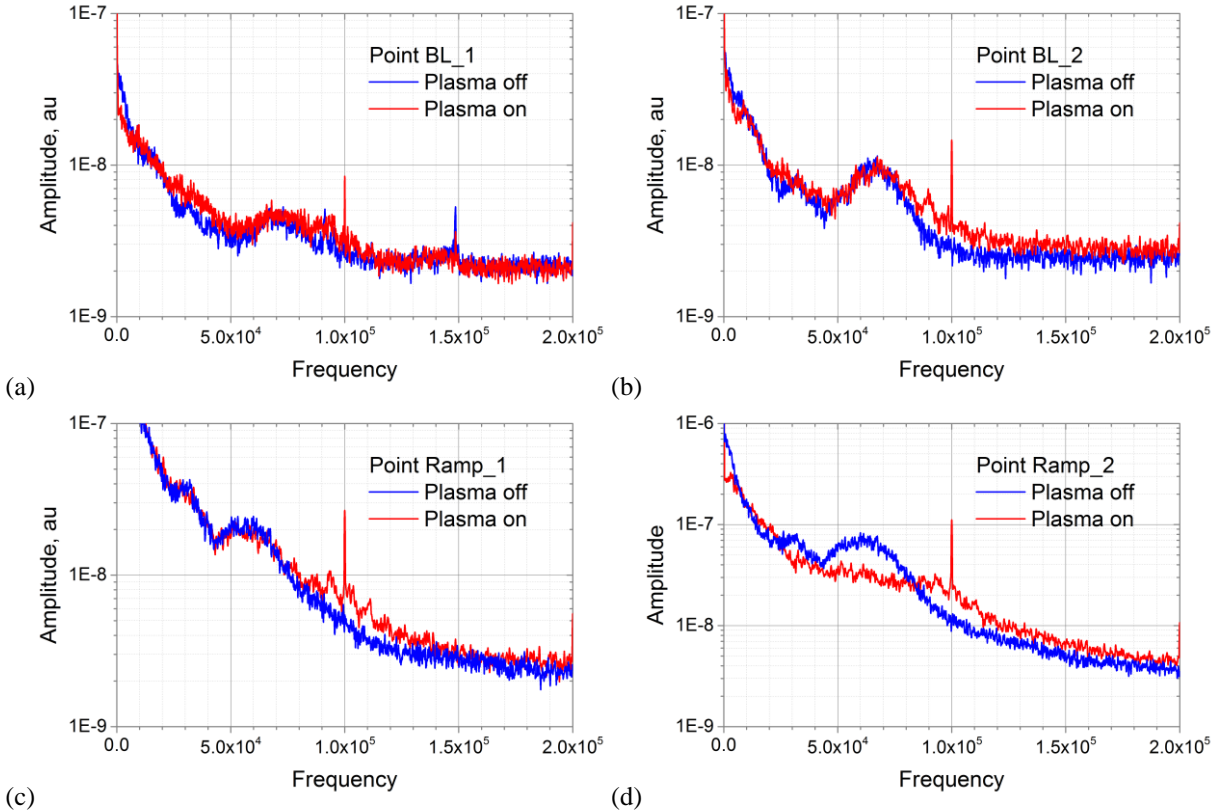
13

Figure 19. Spectra of flow disturbances. Y-component of the deflection-angle spectra, plasma excitation $f = 100\ kHz$, over 25° compression ramp.

IV. Conclusion

The M=4.5 high speed flow structure over the model with 20° and 25° compression ramps has been characterized for low enthalpy (T0=300K) and high enthalpy (T0>800K) conditions and at impact of two pulse periodic plasma generators installed upstream of the compression ramp. Plasma generators possess a low average power in a range of W_{av}=80-300W but at rather different frequencies of repetition: F=5 kHz for a Three-Electrodes Discharge vs F=100kHz for a Shallow Cavity Discharge. Flow characterization was performed through the measurement performed by four methods: a high frequency Shack Hartmann wavefront sensor, schlieren system, Kulite pressure transducers, and high frequency PCB pressure sensors. Through flow characterization, the determination of dominant natural frequencies within the flow were provided experimentally and compared to acoustic wave frequency estimations. An upward shift of dominant frequencies was observed in pressure spectra as Re number was increased. Shack Hartmann data also shows an amplification of naturally occurring acoustic type waves as the flow travels downstream. As expected, the frequency of these waves decreases as the flow perturbations are amplified in locations further downstream.

Through both methods of plasma actuation explored in this study, evidences of changes in dominant flow perturbation frequencies from their natural state occur in the region of separation over a compression ramp in Mach 4.5 flow. These changes can be described as an amplification or reduction of the perturbations at certain frequencies, which is often observed as a shift in the dominant frequency peaks from the natural state. During TED operation, plasma pulses occurring at 5 kHz lead to well-observed modification in the spectra of perturbations occurring in the separation zone over a 20° ramp. Spectra calculated from the pressure data gathered by PCB sensors show a downward shift in high frequency dominant acoustic peaks within the separation zone during plasma actuation. During SCD operation at a 100 kHz pulsing rate, aero-optical data consistently indicates an excitation of flow perturbations just above naturally occurring acoustic waves both within the separation zone and boundary-layer upstream.

14

The plausibility of a controlling effect exerted by a pulsed plasma on the flow in a corner separation zone is given through an estimate of the receptivity and amplification of flow perturbations appearing there. Measurements made by a Shack-Hartmann wavefront sensor show spatially and temporally resolved density fluctuations in the flow, indicating changes in the flow due to plasma actuation. Processing and analysis of schlieren images provides spectral data as well, indicating that at lower frequency plasma pulsing rates, the separation zone experiences a corresponding oscillation effect as well. While spectral data from these optical methods are the result of measurements in the density gradient within the flow, pressure perturbations at the surface were measured by surface mounted sensors demonstrating a consistent result.

As the nature of this study included a first look at various measurements of perturbations induced by these two methods of plasma actuation, further testing of this model will continue, with efforts to characterize the dynamics of flow perturbations with and without plasma actuation for a wider range of repetition frequencies and plasma power deposition. Analysis of data collected by pressure sensors, Shack-Hartmann sensor, and schlieren method at even higher Re will be possible with future upgrades to the test facility. At higher Re conditions, perturbations may be amplified to a greater extent for clearer observation within the boundary-layer and separation zone.

References

[1] A. Houpt, B. Hedlund, S. Gordeyev, T. J. Juliano and S. B. Leonov, "Transient Plasma Impact on Spectra of Flow Disturbances in a Corner Separation Zone at Mach 4.5," in *47th AIAA Plasmadynamics and Lasers Conference* , 2016 Paper *AIAA-2016-4304*.

[2] S.-k. Im, L. Wermer, D. Baccarella, Q. Liu, B. McGann and H. Do, "Ramp Separation Response to Laser-Induced Breakdown Disturbed Boundary Layer at M=4.5," AIAA Paper 2016-0616.

[3] S. A. Berry, R. J. Nowak and T. J. Horvath, "Boundary Layer Control for Hypersonic Airbreathing Vehicles," in *34th AIAA Fluid Dynamics Conference,* AIAA Paper 2004-2246, Portland, Oregon, 28 June-1 July, 2004.

[4] S. Schneider, "Effects of Roughness on Hypersonic Boundary-Layer Transition," *Journal of Spacecraft and Rockets,* vol. 45, no. 2, pp. 193-209, 2008.

[5] E. Reshotko and A. Tumin, "Role of Transient Growth in Roughness-Induced Transition," *AIAA Journal,* vol. 42, no. 4, pp. 766-770, April 2004.

[6] H. Yan and D. Gaitonde, "Effect of Thermally Induced Perturbation in Supersonic Boundary Layers," *Physics of Fluids,* vol. 22, no. 064101, pp. 1-17, 2010.

[7] S. Leonov, A. Houpt and F. Falempin, "Control of Hypersonic BL Transition by Electrical Discharge (feasibility study)," AIAA Paper 2015-3602 in *20th AIAA International Space Planes and Hypersonic Systems and Technologies Conference*, Glasgow, Scotland, 2015.

[8] J. Kriegseis, B. Simon, S. Grundmann, "Towards In-Flight Applications? A Review on Dielectric Barrier Discharge-Based Boundary-Layer Control," *Applied Mechanics Reviews*, Vol. 68, 020802-1, 2016.

[9] S. Leonov, I. Adamovich, and V. Soloviev, "Dynamics of Near-Surface Electric Discharges and Mechanisms of their Interaction with the Airflow," *Plasma Sources Science and Technology,* Vol. 25, 063001, 2016.

[10] M. Kotsonis, "Diagnostics for Characterization of Plasma Actuators," *Measurement Science and Technology*, Vol. 26, 092001, 2015.

[11] K. Choi, T. Jukes, R. Whalley, "Turbulent Boundary-layer Control with Plasma Actuators," *Philosophical Transactions of the Royal Society A: Mathematical, Physical& Engineering Sciences,* Vol. 369(1940), pp. 390-401, 2011.

[12] J. Sontag and S. Gordeyev, "Non-intrusive Velocity and Density Measurements in Subsonic Turbulent Boundary Layer," AIAA Paper 2015-3247 in *46th AIAA Plasmadynamics and Lasers Conference*, Dallas, Texas, 2015.

[13] K. R. Raman, "Surface Pressure Fluctuations in Hypersonic Turbulent Boundary Layers," NASA CR-2386, February 1974.

15

[14] M. Estorf, et al., "Surface-Pressure Measurements of Second-Mode Instability in Quiet Hypersonic Flow," AIAA Paper 2008-1153, 2008.

[15] R. K. Tyson, Principles of Adaptive Optics, New York: Academic., 1997.

[16] J. Sontag and S. Gordeyev, "Non-intrusive Velocity and Density Measurements in Subsonic Turbulent Boundary Layer," in *46th AIAA Plasmadynamics and Lasers Conference*, Dallas, Texas, 2015.

[17] K. D. Bayoda, N. Benard and E. Moreau, "Nanosecond pulsed sliding dielectric barrier discharge plasma actuatorair for airflow control: Electrical, optical, and mechanical characteristics," J. Appl. Phys., vol. 118, p. 063301, 2015.

[18] H. Nishida and T. Shiraishi, "Experimental Characterization of Dual-Grounded Tri-Electrode Plasma Actuator," AIAA Journal, vol. 53, no. 11, pp. 3483-3487, 2015.

[19] S. Leonov, A. Houpt and F. Falempin, "Control of Hypersonic BL Transition by Electrical Discharge (feasibility study)," in AIAA Paper 2015-3602, 2015.

[20] A. Houpt, S. Leonov, S. Gordeyev and T. Juliano, "Optical Measurement of Transient Plasma Impact on Corner Separation in M=4.5 Airflow," Paper AIAA-2016-2160.

[21] A.E. Smith, S. Gordeyev, H. Ahmed, A. Ahmed, D.J. Wittich III and M. Paul, "Shack-Hartmann Wavefront Measurements of Supersonic Turbulent Boundary Layers in the TGF," AIAA Paper 2014-2493

[22] S. Gordeyev, A. E. Smith, J.A. Cress and E.J. Jumper, "Experimental studies of aero-optical properties of subsonic turbulent boundary layers", Journal of Fluid Mechanics, 740, pp. 214-253, 2014

[23] M. Choudhari, F. Li and J. Edwards, "Stability Analysis of Roughness Array Wake in a High-Speed Boundary Layer," in 47th AIAA Aerospace Sciences Meeting, AIAA-2009-170, Orlando, Florida, 5-8 January, 2009.